

Scalar generalized nonlinear Schrödinger equation-quantified continuum generation in an all-normal dispersion photonic crystal fiber for broadband coherent optical sources

Haohua Tu,^{1,*} Yuan Liu,¹ Jesper Lægsgaard,² Utkarsh Sharma,¹ Martin Siegel,³ Daniel Kopf,³ and Stephen A. Boppart¹

¹*Biophotonics Imaging Laboratory, Beckman Institute for Advanced Science and Technology, University of Illinois at Urbana-Champaign, Urbana, Illinois 61801, USA*

²*DTU Fotonik - Department of Photonics Engineering, Technical University of Denmark, DK-2800 Kgs. Lyngby, Denmark*

³*High Q Laser Innovation GmbH, Feldgut 9, A-6830 Rankweil, Austria*

*htu@illinois.edu

Abstract: We quantitatively predict the observed continuum-like spectral broadening in a 90-mm weakly birefringent all-normal dispersion-flattened photonic crystal fiber pumped by 1041-nm 229-fs 76-MHz pulses from a solid-state Yb:KYW laser. The well-characterized continuum pulses span a bandwidth of up to 300 nm around the laser wavelength, allowing high spectral power density pulse shaping useful for various coherent control applications. We also identify the nonlinear polarization effect that limits the bandwidth of these continuum pulses, and therefore report the path toward a series of attractive alternative broadband coherent optical sources.

©2010 Optical Society of America

OCIS codes: (190.4370) Nonlinear optics, fibers; (060.5295) Photonic crystal fibers; (320.6629) Supercontinuum generation; (320.5520) Pulse compression; (320.5540) Pulse shaping; (060.2420) Fibers, polarization-maintaining.

References and links

1. J. K. Ranka, R. S. Windeler, and A. J. Stentz, "Visible continuum generation in air-silica microstructure optical fibers with anomalous dispersion at 800 nm," *Opt. Lett.* **25**(1), 25–27 (2000).
2. J. M. Dudley, and J. R. Taylor, "Ten years of nonlinear optics in photonic crystal fibre," *Nat. Photonics* **3**(2), 85–90 (2009).
3. Y. Silberberg, "Quantum coherent control for nonlinear spectroscopy and microscopy," *Annu. Rev. Phys. Chem.* **60**(1), 277–292 (2009).
4. U. Morgner, F. X. Kärtner, S. H. Cho, Y. Chen, H. A. Haus, J. G. Fujimoto, E. P. Ippen, V. Scheuer, G. Angelow, and T. Tschudi, "Sub-two-cycle pulses from a Kerr-lens mode-locked Ti:sapphire laser," *Opt. Lett.* **24**(6), 411–413 (1999).
5. T. R. Schibli, O. Kuzucu, J.-W. Kim, E. P. Ippen, J. G. Fujimoto, F. X. Kaertner, V. Scheuer, and G. Angelow, "Toward single-cycle laser systems," *IEEE J. Sel. Top. Quantum Electron.* **9**(4), 990–1001 (2003).
6. F. Druon, and P. Georges, "Pulse-compression down to 20 fs using a photonic crystal fiber seeded by a diode-pumped Yb:SYS laser at 1070 nm," *Opt. Express* **12**(15), 3383–3396 (2004).
7. B. Schenkel, R. Paschotta, and U. Keller, "Pulse compression with supercontinuum generation in microstructure fibers," *J. Opt. Soc. Am. B* **22**(3), 687–693 (2005).
8. B. von Vacano, T. Buckup, and M. Motzkus, "Shaper-assisted collinear SPIDER: fast and simple broadband pulse compression in nonlinear microscopy," *J. Opt. Soc. Am. B* **24**(5), 1091–1100 (2007).
9. A. A. Amorim, M. V. Tognetti, P. Oliveira, J. L. Silva, L. M. Bernardo, F. X. Kärtner, and H. M. Crespo, "Sub-two-cycle pulses by soliton self-compression in highly nonlinear photonic crystal fibers," *Opt. Lett.* **34**(24), 3851–3853 (2009).
10. A. Sell, G. Krauss, R. Scheu, R. Huber, and A. Leitenstorfer, "8-fs pulses from a compact Er:fiber system: quantitative modeling and experimental implementation," *Opt. Express* **17**(2), 1070–1077 (2009).
11. J. M. Dudley, G. Genty, and A. Coen, "Supercontinuum generation in photonic crystal fiber," *Rev. Mod. Phys.* **78**(4), 1135–1184 (2006).
12. A. V. Husakou, and J. Herrmann, "Supercontinuum generation of higher-order solitons by fission in photonic crystal fibers," *Phys. Rev. Lett.* **87**(20), 203901 (2001).

13. T. Südmeyer, F. Brunner, E. Innerhofer, R. Paschotta, K. Furusawa, J. C. Baggett, T. M. Monro, D. J. Richardson, and U. Keller, "Nonlinear femtosecond pulse compression at high average power levels by use of a large-mode-area holey fiber," *Opt. Lett.* **28**(20), 1951–1953 (2003).
14. G. McConnell, and E. Riis, "Ultra-short pulse compression using photonic crystal fibre," *Appl. Phys. B* **78**(5), 557–563 (2004).
15. N. Nishizawa, and J. Takayanagi, "Octave spanning high-quality supercontinuum generation in all-fiber system," *J. Opt. Soc. Am. B* **24**(8), 1786–1792 (2007).
16. A. M. Heidt, "Pulse preserving flat-top supercontinuum generation in all-normal dispersion photonic crystal fibers," *J. Opt. Soc. Am. B* **27**(3), 550–559 (2010).
17. H. Wang, C. P. Fleming, and A. M. Rollins, "Ultrahigh-resolution optical coherence tomography at 1.15 μm using photonic crystal fiber with no zero-dispersion wavelengths," *Opt. Express* **15**(6), 3085–3092 (2007).
18. T. P. White, B. T. Kuhlmeier, R. C. McPhedran, D. Maystre, G. Renversez, C. M. de Sterke, and L. C. Botten, "Multipole method for microstructured optical fibers. I. Formulation," *J. Opt. Soc. Am. B* **19**(10), 2322–2330 (2002).
19. M. J. Steel, T. P. White, C. Martijn de Sterke, R. C. McPhedran, and L. C. Botten, "Symmetry and degeneracy in microstructured optical fibers," *Opt. Lett.* **26**(8), 488–490 (2001).
20. K. J. Blow, and D. Wood, "Theoretical description of transient stimulated Raman scattering in optical fibers," *IEEE J. Quantum Electron.* **25**(12), 2665–2673 (1989).
21. B. Washburn, S. Ralph, and R. Windeler, "Ultrashort pulse propagation in air-silica microstructure fiber," *Opt. Express* **10**(13), 575–580 (2002).
22. D. V. Skryabin, F. Luan, J. C. Knight, and P. St. J. Russell, "Soliton self-frequency shift cancellation in photonic crystal fibers," *Science* **301**(5640), 1705–1708 (2003).
23. J. Dudley, X. Gu, L. Xu, M. Kimmel, E. Zeek, P. O'Shea, R. Trebino, S. Coen, and R. Windeler, "Cross-correlation frequency resolved optical gating analysis of broadband continuum generation in photonic crystal fiber: simulations and experiments," *Opt. Express* **10**(21), 1215–1221 (2002).
24. A. Efimov, A. Taylor, F. Omenetto, A. Yulin, N. Joly, F. Biancalana, D. Skryabin, J. Knight, and P. Russell, "Time-spectrally-resolved ultrafast nonlinear dynamics in small-core photonic crystal fibers: Experiment and modelling," *Opt. Express* **12**(26), 6498–6507 (2004).
25. K. L. Corwin, N. R. Newbury, J. M. Dudley, S. Coen, S. A. Diddams, K. Weber, and R. S. Windeler, "Fundamental noise limitations to supercontinuum generation in microstructure fiber," *Phys. Rev. Lett.* **90**(11), 113904 (2003).
26. D. R. Solli, C. Ropers, P. Koonath, and B. Jalali, "Optical rogue waves," *Nature* **450**(7172), 1054–1057 (2007).
27. M. H. Frosz, "Validation of input-noise model for simulations of supercontinuum generation and rogue waves," *Opt. Express* **18**(14), 14778–14787 (2010).
28. G. P. Agrawal, *Nonlinear Fiber Optics*, 4th edition (Academic Press, Boston, 2007), Chap. 2.
29. H. Tu, X. Liang, D. L. Marks, and S. A. Boppart, "Emergence of self-organized long-period fiber gratings in supercontinuum-generating optical fibers," *Opt. Lett.* **34**(5), 668–670 (2009).
30. H. Tu, S. Shin, R. John, and S. A. Boppart, "Long-period fiber gratings spontaneously written by a mechanism markedly different from Hill grating formation," *Appl. Phys. Lett.* **97**(12), 121104 (2010).
31. R. Sai Santosh Kumar, K. L. N. Deepak, and D. Narayana Rao, "Control of the polarization properties of the supercontinuum generation in a noncentrosymmetric crystal," *Opt. Lett.* **33**(11), 1198–1200 (2008).
32. B. Kibler, J. M. Dudley, and S. Coen, "Supercontinuum generation and nonlinear pulse propagation in photonic crystal fiber: influence of the frequency-dependent effective mode area," *Appl. Phys. B* **81**(2-3), 337–342 (2005).
33. B. B. Xu, J. M. Gunn, J. M. D. Cruz, V. V. Lozovoy, and M. Dantus, "Quantitative investigation of the multiphoton intrapulse interference phase scan method for simultaneous phase measurement and compensation of femtosecond laser pulses," *J. Opt. Soc. Am. B* **23**(4), 750–759 (2006).
34. Y. Coello, V. V. Lozovoy, T. C. Gunaratne, B. Xu, I. Borukhovich, C. Tseng, T. Weinacht, and M. Dantus, "Interference without an interferometer: a different approach to measuring, compressing, and shaping ultrashort laser pulses," *J. Opt. Soc. Am. B* **25**(6), A140–A150 (2008).
35. D. Turchinovich, X. Liu, and J. Laegsgaard, "Monolithic all-PM femtosecond Yb-fiber laser stabilized with a narrow-band fiber Bragg grating and pulse-compressed in a hollow-core photonic crystal fiber," *Opt. Express* **16**(18), 14004–14014 (2008).
36. X. Liu, J. Laegsgaard, and D. Turchinovich, "Highly-stable monolithic femtosecond Yb-fiber laser system based on photonic crystal fibers," *Opt. Express* **18**(15), 15475–15483 (2010).
37. J. T. Kristensen, A. Houmann, X. Liu, and D. Turchinovich, "Low-loss polarization-maintaining fusion splicing of single-mode fibers and hollow-core photonic crystal fibers, relevant for monolithic fiber laser pulse compression," *Opt. Express* **16**(13), 9986–9995 (2008).

1. Concept of alternative coherent broadband optical sources

White-light generation by the combination of a photonic crystal fiber (PCF) and an oscillator-type ultrafast laser was reported in 2000 [1], and has since initiated the so-called supercontinuum revolution [2]. One decade later, however, the apparent promise of the fiber continuum as a coherent broadband compressible pulsed source amendable for arbitrary pulse shaping remains largely unfulfilled. Such source is indispensable in coherent control ultrafast spectroscopy and microscopy [3], but is technically challenging in the form of mode-locked

solid state lasers [4,5]. To generate near transform-limited (TL) <15 fs fiber continuum pulses, it has been considered beneficial to select a short (<10 mm) fiber length, a short (<50 fs) incident laser pulse, an adequately low (<2 nJ) pulse energy transmitting in the fiber, a particularly filtered spectral range of the continuum, or combinations of the four [6–10] (Table 1). None of these restrictions are practically desirable due to difficulty in fiber-handling, laser complexity, and low power throughput. We note that all these restrictions are intended to improve the coherence of the continuum conventionally generated by a PCF having a zero-dispersion-wavelength (ZDW) located inside the spectral range of the continuum [11]. The reason such zero-dispersion PCF is of interest is because it can invoke soliton dynamics to generate the broadest continuum [12], which in principle, could lead to the shortest pulse. However, in order to develop a practical and useful coherent broadband fiber source, it is advantageous to perform the entire spectral broadening in a normal dispersion region of the fiber [13,14], and therefore remove all these restrictions [11]. Fiber continuum generation in a normal dispersion region of the fiber has been known to be highly coherent [11,15,16].

Table 1. Representative compressible fiber continua as broadband coherent optical sources

Reference	[6]	[7]	[8]	[9]	[10]	[13]	[14]
Fiber: type polarization ZDW nonlinearity length	PCF PM 1065 nm low 200 mm	PCF non-PM 790 nm medium 5 mm	PCF PM 800 nm medium 24 mm	PCF non-PM 670 nm high 4.85 mm	circular non-PM 1540 nm medium 4.5 mm	PCF non-PM 1250 nm low 170 mm	PCF non-PM 900 nm medium 86 mm
Input pulse: pulse width wavelength pulse energy repetition rate gain medium	100-fs 1070-nm 4-nJ 98-MHz Yb:SYS	15-fs 790-nm 12-nJ 19-MHz Ti:Sa	100-fs 807-nm 3-nJ 80-MHz Ti:Sa	41-fs 816-nm 2-nJ 85-MHz Ti:Sa	70-fs 1550-nm 5-nJ 49-MHz Er:fiber	810-fs 1030-nm 1.3- μ J 34-MHz Yb:YAG	250-fs 830-nm 4-nJ 80-MHz Ti:Sa
Method of compression	prism pair	SLM	SLM	fiber itself	prism pair	prism pair	grating pair
Output pulse: pulse width pulse energy coherence TBP quality	20-fs 0.3-nJ unclear fair	5.5-fs 0.2-nJ unclear very good	14.4-fs 0.3-nJ unclear excellent	4.6-fs 0.46-nJ unclear fair	7.8-fs 0.7-nJ unclear good	33-fs 0.53 μ J high good	25-fs 0.3-nJ high good
Advantages	long fiber, compact pump laser	short pulse, good TBP	good TBP	short pulse, efficient, simple	short pulse, compact fiber format	long fiber, high power	long fiber, simple setup
Limitations	long pulse, sidelobe present at high- power pumping	short fiber, low power, prechirp pumping	pulse width difficult to shorten further	short fiber, prechirp pumping, far from TL	spectral filtering, prechirp pumping, prechirp fiber	long pulse, sidelobe, possible PCF damage	long pulse, sidelobe, pulse width limited by ZDW of PCF

TBP: time-bandwidth product; PM: polarization-maintaining; SLM: spatial light modular; TL: transform limited.

For normal dispersion spectral broadening, the pulse duration (or equivalently, bandwidth) of the compressed pulses has been limited by either the low nonlinearity [13] or the blue shifted ZDW [14] of the fiber (Table 1). The low nonlinearity is not an intrinsic limitation if a high-power pump laser is available. Neither is the blue shifted ZDW because the powerful dispersion engineering capability of the PCF permits the fabrication of the fiber with no ZDW in its optical transmission window [17]. This fact can be easily verified by considering a typical pure silica PCF, whose cross section consists of multiple (>5) layers of hexagonal arranged circular holes but misses the central hole (Fig. 1, inset). The dispersion β_2 of such fiber can be calculated by a multipole method [18] for given values of pitch A (i.e., hole-to-hole distance) and hole diameter d . For carefully chosen A and d values, flattened and decreased all-normal dispersion profiles can be obtained around 800 nm, 1040 nm, and 1250

nm, corresponding respectively to the typical wavelength of a Ti:sapphire laser, a Yb-based laser, and a Cr:forsterite laser (Fig. 1). It is therefore rather obvious to employ these combinations of lasers and fibers for developing a series of alternative coherent broadband optical sources, replacing the complex ultrabroadband mode-locked solid state lasers, or the conventional ZDW PCF-based continuum sources with possibly imperfect coherence.

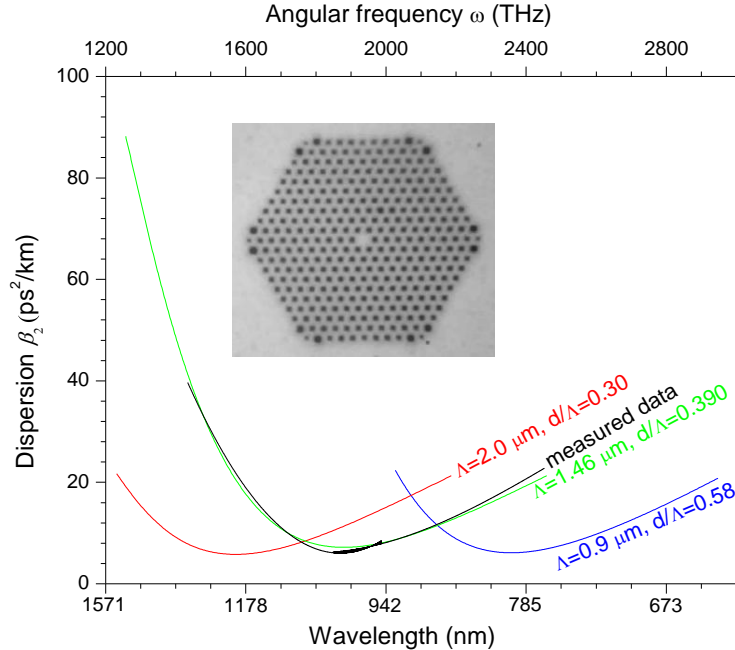


Fig. 1. Calculated dispersion curves of a hexagonal PCF for given structural parameters of Λ and d/Λ (red, green, and blue curves), and measured dispersion curve of the hexagonal PCF under investigation in this study (black curve). The inset shows the scanning electron microscopy image of the PCF with the measured dispersion curve.

With their distinguishable dispersion profiles, the fibers employed in this series of alternative coherent broadband sources can be termed as dispersion-flattened dispersion-decreased all-normal dispersion fibers (DFDD-ANDiF). This concept of high-quality continuum sources based on a DFDD-ANDiF has been proposed for the pump laser wavelength around 1080 nm [16], and experimentally demonstrated in the telecommunication wavelength region around 1550 nm [15]. In sharp contrast to these two studies, here we find out experimentally that the most straightforward method to implement an alternative coherent broadband source should avoid the non-birefringent DFDD-ANDiF with a guiding core of circular, hexagonal, or other types of high-order rotational symmetry [19]. Rather, a certain degree of asymmetry should be intentionally introduced to the DFDD-ANDiF to attain a linear modal birefringence of $>2 \times 10^{-5}$. Somewhat surprisingly, this finding relies on the rigorous quantification of the spectral broadening in a DFDD-ANDiF based on the scalar generalized nonlinear Schrödinger equation (GNLSE) [11,20].

2. Quantification of fiber continuum generation by the scalar GNLSE

The scalar GNLSE has qualitatively or semi-quantitatively explained a range of unusual nonlinear fiber optics phenomena, including soliton self-frequency shift and associated dispersive wave generation [10,21], soliton self-frequency shift cancelation [22], X-FROG spectrogram evolution [23,24], relative intensity noise of fiber continuum [25], and optical

rogue waves [26]. Thus, one would expect it to quantitatively predict the spectral-temporal properties of fiber continuum pulses, which in turn could guide the pulse compression to develop useful broadband coherent sources. Ironically, few reports have rigorously quantified an observed fiber continuum (with more than 200 nm bandwidth) and unambiguously reproduced all of its spectral features in the linear intensity scale. As a result, the pulse compression of most fiber continua is more like art than science. This raises a valid question whether the derivation of the scalar GNLSE from Maxwell's equations contains certain oversimplifications, or the experiments of fiber continuum generation are not well-controlled.

The continuum generation in a relatively short (~ 100 mm) DFDD-ANDiF can be considered as an ideal case to address this question. First, the continuum generation does not invoke solitons so that the noise term in the scalar GNLSE can be ignored. This is an important simplification since the inclusion of the noise model is nontrivial [27]. Second, the self-phase modulation-related spectral fringes presented at short fiber lengths [13,16] can offer rich spectral structures to test the scalar GNLSE, while the linear loss of the fiber can be safely neglected. Considering these simplifications, we can write the scalar GNLSE as

$$\frac{\partial U(z, T)}{\partial z} - \sum_{k \geq 2} \frac{i^{k+1} \beta_k}{k!} \frac{\partial^k U(z, T)}{\partial T^k} = \frac{1}{L_{NL}} \left(i - \frac{1}{\omega_0} \frac{\partial}{\partial T} \right) \left(U(z, T) \int_{-\infty}^{\infty} R(T') |U(z, T-T')|^2 dT' \right) \quad (1)$$

In Eq. (1), $U(z, T)$ is the normalized pulse envelope by the square root of the peak power of the incident pulses (i.e., $\sqrt{P_0}$), which is a function of propagation fiber length z and the retarded time frame T moving with the pulse at the group velocity, ω_0 is the angular frequency of the incident pulse, and L_{NL} is the nonlinear length that can be calculated from $1/(\gamma P_0)$, where γ is the nonlinear coefficient. The left hand side of Eq. (1) models the linear propagation effects characterized by a series of dispersion coefficients β_k . The nonlinear response function $R(t)$ in Eq. (1) can be written as [28]

$$R(t) = (1 - f_R) \delta(t) + f_R \frac{\tau_1^2 + \tau_2^2}{\tau_1 \tau_2} \exp\left(-\frac{t}{\tau_2}\right) \sin\left(\frac{t}{\tau_1}\right) \quad (2)$$

The first term and the second term on the right hand side of Eq. (2) represent the contribution of the instantaneous electronic response and delayed Raman response, respectively.

3. Experiment

Our setup of fiber continuum generation was specifically designed to facilitate the calculation of Eq. (1) with minimum uncertainties (Fig. 2). We selected a recently developed solid-state Yb:KYW laser (FemtoTRAIN, High-Q laser GmbH, Austria) as the pump laser. The new cavity design allows the directly diode-pumped laser to be both compact and environmental stable. The laser generated linearly polarized 1041-nm 76-MHz pulses with an average power of 3.7 W. It emits transform-limited soliton-type pulses by design, so that the envelope of the pulses is a secant hyperbolic function $\text{sech}(T/T_0)$ defined by the pulse width T_0 , which is 0.567 times the FWHM pulse width. We used a lab-built autocorrelator to measure the FWHM width of the pulses directly from the laser, yielding a value of 229 ± 5 fs, which is consistent with the manufacture-specified value of 220 fs. This measurement assigned a value of 130 ± 3 fs to T_0 . The laser pulses were dispersed by an optical isolator, a neutral-density filter-type attenuator, and a half wave plate (for controlling the polarization of the incident pulses), before being focused by an aspheric lens (C330TME-C, Thorlabs, Newton, NJ) on the fiber end-face. Due to the thinness of the aspheric lens, the dispersion of the laser pulses should be dominated by the three dispersive optical components in front of the aspheric lens, particularly the terbium gallium garnet crystal-based optical isolator. We used the same autocorrelator to measure the FWHM width of the dispersed pulses immediately before the aspheric lens (Fig. 2), and obtained a value of 283 fs. Such pulse elongation corresponds to a

linear positive chirp of 8500 fs^2 . Thus, the envelope of the laser pulses directly incident on the fiber was well-defined.

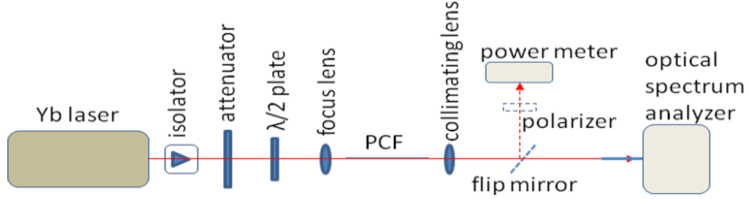


Fig. 2. Schematic of PCF continuum generation and corresponding measurements.

We selected a DFDD-ANDiF (NL-1050-NEG-1, NKT Photonics, Denmark). The cross-sectional scanning electron microscopy image of the fiber is shown in the inset of Fig. 1. The dispersion profile of the fiber was measured by the manufacturer (Fig. 1), presumably by spectral white-light interferometry. The measured profile approximates that of the theoretical dispersion profile corresponding to the fiber parameters of $\Lambda = 1.46 \pm 0.02 \mu\text{m}$ and $d/\Lambda = 0.390 \pm 0.005$ (Fig. 1). This agreement permits the accurate determination of the dispersion coefficients β_k . We note that the above selection of the pump laser and the fiber leaves little uncertainty in Eq. (1).

The aspheric lens and the PCF were mounted on a standard fiber launcher. The average power of the incident laser beam was attenuated below 1 W before it was launched into the fiber. Higher incident powers could undesirably produce a self-organized long-period fiber grating inside the fiber [29,30]. The coupling efficiency was $\sim 55\%$, and had little dependence on the incident power, incident beam polarization, fiber length, and individual cleave. Thus, the fiber output power was up to 0.55 W. The continuum generated from the fiber was collimated by another identical aspheric lens to enter a fiber-coupled optical spectrum analyzer (86140B, Agilent Technologies), which recorded the spectrum of the continuum as a function of the fiber output power, measured separately by a power meter (Fig. 2). The spectral resolution of the optical spectrum analyzer was set at 1 nm to resolve the finest spectral features of the continuum. The polarization property of the continuum could be studied by placing a broadband (650-2000 nm) polarizer before the power meter (Fig. 2).

4. Results

4.1 Characterization of fiber linear birefringence

Under a wide range of fiber lengths and the incident powers (0.2-1 W), the spectrum of the continuum generated from the PCF was found out to depend sensitively on the polarization of the incident laser beam. Rotating the half wave plate before the aspheric lens (Fig. 2) did not change the power of the continuum, but noticeably changed the spectrum of the continuum, particularly at high incident powers. Also, the continuum was rather unpolarized, particularly at long fiber lengths and high incident powers. These facts make it impossible to compare the observed spectrum of fiber continuum with the calculated spectrum from the scalar GNLSE.

To avoid the random birefringence associated with fiber bending, we straightly mounted a PCF with a relatively short length of $\sim 200 \text{ mm}$, and operated the Yb:KYW laser in CW mode at a constant power ($\sim 0.1 \text{ W}$) to investigate the nature of the fiber birefringence within the scope of linear optics. The fiber coupling efficiency of the CW laser beam approximated that of the pulsed beam, and was insensitive to the rotation of the half wave plate. Varying the polarization of the incident CW beam by the half wave plate while measuring the polarization extinction ratio (PER) of the fiber output by the polarizer and the power meter (Fig. 2), we always identified two orthogonal polarization orientations of the incident CW beam to maximize the PER of the fiber output at around 20 dB, which was limited by the dynamic range of the power meter. Also, the two polarization orientations of the highly polarized fiber output corresponding to the two orthogonal polarization orientations of the incident CW beam was also orthogonal to each other. These evidences indicate that the PCF has two principal

axes along which linearly polarized CW light remains linearly polarized, i.e., such a short length PCF can be treated as a linearly birefringent fiber with no detectable elliptical birefringence.

With the two principal axes of the PCF identified, we oriented the polarization of the incident CW beam at 45° between the two axes, and used fiber cut-back at 10 mm intervals to measure the periodicity of the polarization pattern of the fiber output, i.e., the beat length. The measured beat length was 80 mm, with ± 30 mm variation among different ~200-mm PCFs. This beat length corresponds to a linear birefringence of $1.5 \pm 0.6 \times 10^{-5}$ at 1041-nm wavelength. Since the core diameter of the PCF was only 2.3 μm , the inherently unintentional structural symmetry breaks during the fiber fabrication could lead to such linear birefringence at short fiber lengths. This type of unintentional birefringence could be present in a wide variety of nonlinear PCFs, including the supercontinuum-generating ZDW PCFs.

4.2 Observation of nonlinear polarization-mode depolarization

The above cut-back method of birefringence measurement left a PCF with a linear birefringence of 1.9×10^{-5} and a length of 90.0 mm. Since the principal axes of the PCF were identified, we operated the Yb:KYW laser in regular mode-locking mode, and oriented the polarization of the incident pulses along one of the two axes. To quantify the extent of possible polarization-mode depolarization, we oriented the polarizer along the same principal axis at the fiber exiting end to measure the output power P_{\parallel} , and also along its orthogonal axis to measure the output power P_{\perp} . The extent of the depolarization can be represented by $P_{\perp}/(P_{\perp} + P_{\parallel})$. Figure 3 shows the measured extent of the depolarization as a function of fiber output power corresponding to either of the two principal axes of the PCF. At low fiber output powers (<0.08 W), the extent of the depolarization of either principal axis is small, approximating that of the CW light. However, nonlinear polarization-mode depolarization onset (taken at an extent of the depolarization of 0.05) occurs at 0.08 W for one principal axis, termed as the weak polarization-maintaining axis, and at 0.36 W for the other principal axis, termed as the strong polarization-maintaining axis. These data are not very sensitive to the polarization of incident pulses within $\pm 3^\circ$ around the principal axes of the PCF.

It is not our intent to understand the origin of the observed nonlinear polarization-mode depolarization, which requires the use of the vector-based GNLSE. However, this effect does indicate the applicability of the scalar GNLSE. Since the scalar GNLSE assumes polarized fiber output from polarized pump input, the corresponding fiber continuum generation experiments should pump the fiber along the strong polarization-maintaining axis with powers below the nonlinear polarization-mode depolarization onset. To examine the dependence of the nonlinear polarization-mode depolarization onset on the linear birefringence of the PCF, the cut-back method for birefringence measurements was employed to obtain another PCF with a linear birefringence of 1.1×10^{-5} and a length of 90.6 mm. For this PCF, the measured extent of the depolarization as a function of fiber output power corresponding to the strong polarization-maintaining axis is also plotted in Fig. 3. The nonlinear polarization-mode depolarization onset is attained at 0.29 W, significantly smaller than that of the first PCF. This evidence indicates that a larger linear birefringence is beneficial for delaying the nonlinear polarization-mode depolarization onset, and therefore for enhancing the applicability of the scalar GNLSE. Similar control of the polarization properties of the supercontinuum generation has been demonstrated in a noncentrosymmetric crystal [31].

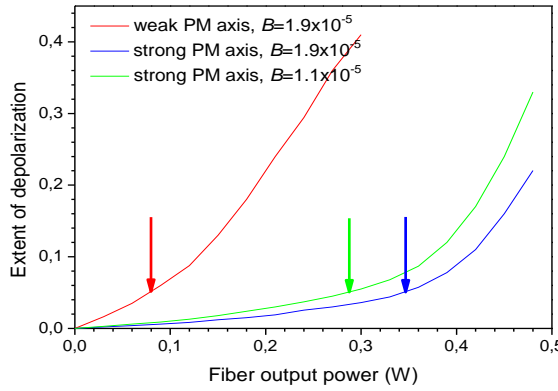


Fig. 3. Extent of depolarization along either the weak or the strong polarization-maintaining axis as a function of fiber output power at a given fiber birefringence B . The vertical arrows indicate the nonlinear polarization-mode depolarization onsets.

4.3 Comparison between experiment and theory

The above preliminary efforts established the experimental conditions where the scalar GNLSE is valid. Our fiber continuum generation experiments were then conducted on the PCF with a linear birefringence of 1.9×10^{-5} and a length of 90.0 mm. The polarization of the incident laser pulses was set along the strong polarization-maintaining axis of the fiber, and the spectra of the continuum were recorded at fiber output powers of 0.061 W, 0.130 W, 0.225 W, and 0.361 W [Fig. 4(a)–4(d)]. The highly polarized fiber continua allow direct comparison with the theoretical results from the scalar GNLSE.

All parameters used in the numerical simulation of Eq. (1) are summarized in Table 2. The only parameter that has large uncertainty is the nonlinear length $L_{0.361}$ at fiber output power of 0.361 W, which is used as the only adjustable parameter. Once the value of this parameter is assumed, the values of L_{NL} at any fiber output power can be easily derived [Fig. 4(a)–4(d)] because L_{NL} is inversely proportional to the fiber output power. The time window is taken to be 50 times of T_0 while 2^{13} points are used to discretize the temporal window. The standard split step Fourier method [28] is used in the simulation whose convergence is ensured by choosing a step size of <0.3 mm. The theoretically calculated spectra at the four fiber output powers are compared with the corresponding observed spectra [Fig. 4(a)–4(d)], showing a high degree of quantitative agreement. The validity of the scalar GNLSE is rigorously confirmed considering that only one adjustable parameter is used to fit all four spectra.

Table 2. Parameters for simulation of scalar GNLSE based on Eq. (1)

Parameter	Value	Uncertainty	Comments
f_k	0.18	constant	known fractional contribution of Raman to electronic response [28]
τ_1	12.2 fs	constant	known parameter characterizing Raman response of pure silica [28]
τ_2	32 fs	constant	known parameter characterizing Raman response of pure silica [28]
L	90.0 mm	± 0.2 mm	accurately measured fiber length
λ	1041 nm	± 0.5 nm	accurately measured central wavelength of pump laser to calculate ω_0
T_0	130 fs	± 3 fs	pulse width defining soliton temporal profile $\text{sech}(T/T_0)$ of unchirped pump laser pulses; determined from autocorrelation measurements
C	8500 fs^2	$\pm 500 \text{ fs}^2$	initial linear chirp of incident laser pulses determined from autocorrelation measurements
Λ	$1.46 \mu\text{m}$	$\pm 0.02 \mu\text{m}$	PCF structural parameters derived by fitting measured dispersion curve (Fig. 1); are used to derive β_k up to the 5th order, $\beta_2/2! = 1980 \text{ fs}^2/\text{m}$, $\beta_3/3! = -1393 \text{ fs}^3/\text{m}$, $\beta_4/4! = 5113 \text{ fs}^4/\text{m}$, $\beta_5/5! = -2903 \text{ fs}^5/\text{m}$
$L_{0.361}$	1.26 mm		nonlinear length L_{NL} at reference fiber output power of 0.361 W

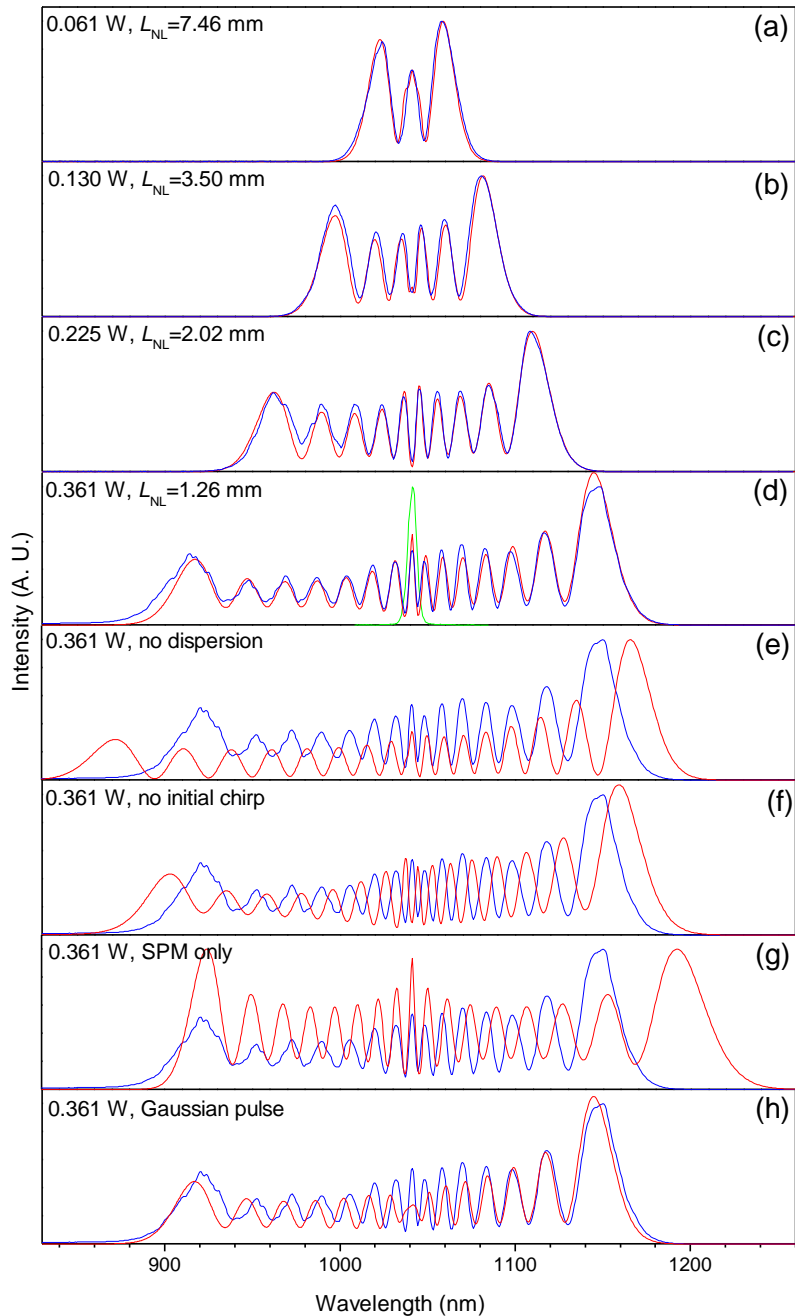


Fig. 4. Comparison of observed (blue curves) and simulated (red curves) fiber continuum spectra of the 90-mm PCF at fiber output powers of 0.061 W, 0.130 W, 0.225 W, and 0.361 W (see text in details). The green curve shows the spectrum of the incident laser pulses.

Another independent method to estimate $L_{0.361}$ is to use the relation of $L_{\text{NL}} = 1/(\gamma P_0)$. The nonlinear coefficient γ can be calculated from the same multipole method that fits the

observed fiber dispersion (Fig. 1), yielding a value of $0.037 \text{ (W}\cdot\text{m)}^{-1}$ at the laser wavelength of 1041 nm. The peak incident power P_0 can be calculated from $P_0 = P/(2T_0R)$, where P is the fiber output power (0.361 W), R is the known repetition rate of the laser pulses (76 MHz), and T_0 is 130 fs. This method results in a $L_{0.361}$ value of 1.48 mm, which is close to the value shown in Table 2. The discrepancy may be attributed to the systematic readout error of the power meter and/or the uncertainty in calculating γ . The merit of writing the scalar GNLSE in the form of Eq. (1) lies in the combination of γ and P_0 into one single parameter L_{NL} , so that the scalar GNLSE can be calculated with a minimum number of parameters (Table 2).

4.4 Aspects of rigorous quantification

The effect of L_{NL} (or equivalently, fiber input power) on the spectrum of the continuum pulses can be appreciated in Fig. 4(a)–4(d). Also, the effect of dispersion can be appreciated by setting all dispersion coefficients β_k in Eq. (1) to zero, and then performing the same simulation [Fig. 4(e)]. Finally, the effect of the initial pulse chirp of 8500 fs^2 can be appreciated by removing this chirp and then performing the same simulation [Fig. 4(f)]. These exercises demonstrate the sensitivity of the continuum spectrum to the parameters of C , Λ , d/Λ , and $L_{0.361}$. Extensive simulations reveal that each value of C , Λ , d/Λ , and $L_{0.361}$ must not deviate by 10% from that given in Table 2 to ensure a high-quality agreement between the simulated and observed spectra if the values of the other parameters in Table 2 are fixed. In other words, the values of these four parameters in Table 2 do not need to be known *a priori*. They can be independently determined with a relative error of less than 10% by simply matching the simulated and observed spectra.

The above sensitivity suggests that the theoretical reproduction of the observed spectral fringes require the scalar GNLSE, not one of its simplified forms. To verify this, we replace the terms on the right hand side of Eq. (1) with a single term that represents the self phase modulation (SPM) [28], and perform the same simulation using the same values of C , Λ , d/Λ , and $L_{0.361}$ [Fig. 4(g)]. Although this simulation largely reproduces the general trend of the spectral fringes, the simulated spectrum deviates substantially from the observed spectrum. Somewhat surprisingly, the observed spectra can be used to discriminate the incident soliton (sech) pulses against Gaussian pulses [Fig. 5(a)]. If the unchirped laser pulses are assumed to have a Gaussian shape with a FWHM of 229 fs, a linear chirp of $1.30 \times 10^5 \text{ fs}^2$ is required to elongate the pulse duration to 283 fs. Using such incident chirped Gaussian pulses to perform the same simulation, we find pronounced disagreement between the simulated and observed spectra [Fig. 4(h)], even though the temporal shape of the incident Gaussian pulses approximates that of the incident soliton pulses [Fig. 5(a)]. All these simulation exercises have demonstrated the usefulness of the SPM-related spectral fringes in the rigorous quantification of the fiber continuum generation. Not surprisingly, at fiber output powers higher than the nonlinear polarization-mode depolarization onset (0.36 W, Fig. 3), significant deviation between the observed and simulated spectra is always found.

5. Discussions

5.1 Remarks on simulating fiber continuum generation by the GNLSE

The main result of this work (Fig. 4) demonstrates the feasibility of rigorous quantification of fiber continuum generation by the scalar GNLSE. Considering the relatively restrictive experimental conditions in use, we believe the lack of such rigorous quantification in the literature is mainly due to the poorly controlled experiments, rather than the oversimplifications in deriving the scalar GNLSE, such as the slowly varying envelope approximation. Although this work reports a rather specific fiber continuum generation, the methodology of the corresponding GNLSE simulation may be generalized to two broader cases. First, the current work may serve as a starting point to understand the nonlinear polarization-mode depolarization using the more advanced tools of the vector-based GNLSE. This will permit quantitative interpretation of unpolarized fiber continuum generation. Second, the same methodology may be applied to conventional supercontinuum generation by

various ZDW PCFs, which have produced the broadest bandwidth. If the incident pulses and the fiber dispersion are well-characterized, the influences of the frequency dependence of modal effective area [32] and the input noise [27] may be quantified independently.

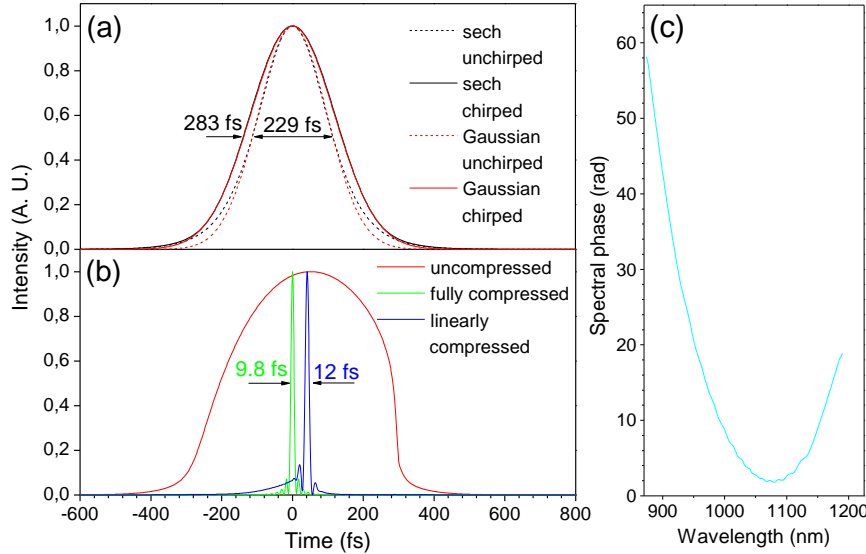


Fig. 5. (a) Temporal profiles of unchirped and chirped incident sech (or Gaussian) pulses with FWHM widths of 229 fs and 283 fs, respectively. (b) Temporal profiles of output continuum pulses at fiber output power of 0.361 W without compression, with compression removing linear chirp, and with compression removing full chirp. (c) Simulated spectral phase of the uncompressed continuum pulses at fiber output power of 0.361 W.

5.2 Pulse compression/shaping of fiber continua

Because the simulated spectrum at fiber output power of 0.361 W is in quantitative agreement with the observed spectrum [Fig. 4(d)], the correspondingly simulated temporal profile [Fig. 5(b)] and the spectral phase [Fig. 5(c)] of the continuum pulses are considered to be quantitatively correct. The temporal profile exhibits a self-steepening at the trailing edge of the pulses, which is likely responsible for the observed asymmetry of spectral broadening [Fig. 4(d)]. Nevertheless, no pulse splitting is observed in the time domain after the spectral broadening, suggesting that the continuum pulses are suitable for pulse compression. The spectral phase of the continuum pulses can be approximated by a linear positive chirp of 680 fs^2 . The removal of this chirp by introducing a compensating linear negative chirp results in a compressed pulse width of 12 fs, approximating the related transform-limited (TL) value of 9.8 fs [Fig. 5(b)]. The pronounced pedestal and sidelobes cannot be prevented by fine tuning the compensating linear negative chirp, indicating the limitation of pulse compression by a prism pair (or grating pair). Consistently, previous attempts to compress similarly generated fiber continua by a grating or prism compressor were unable to compress the pulses close to the TL width [13,14]. More noticeably, the temporal profile of the compressed pulses free of linear chirp [Fig. 5(b)] unusually resembles that measured in Fig. 5 of Ref. 13. These observations reveal the usefulness of the rigorously quantified fiber continua in guiding the pulse compression. In order to compress the continuum pulses close to their TL widths, rigorous quantification asserts that it is necessary to simultaneously remove the linear and nonlinear chirp of the continuum pulses by a spatial light modular (SLM) (Table 1).

One particularly attractive pulse compression/shaping scheme is the combination of the rigorously quantified fiber continuum generation with the multiphoton intrapulse interference phase scan (MIIPS) method for simultaneous phase measurement and compensation of femtosecond laser pulses [33,34]. The rigorously quantified fiber continua allow the calibration of MIIPS-assisted pulse measurement, while the calibrated MIIPS-assisted pulse measurement permits arbitrary pulse measurement and shaping of other unknown pulses spectrally overlapping with the fiber continua. Another attractive pulse compression scheme is the combination of an all-fiber Yb laser-based femtosecond source [35,36] with a SLM-type pulse compressor. The envelope of the femtosecond pulses from the Yb fiber laser, once measured by methods such as cross-correlation frequency-resolved optical grating (X-FROG) or spectral phase interferometry for direct electric-field reconstruction (SPIDER), may produce similarly scalar GNLSE-quantified fiber continua amendable for the flexible pulse compression afforded by the SLM. Thus, the continuum-generating fiber may be spliced directly on the output fiber of the fiber laser [37] for maximum simplicity.

5.3 Routes toward alternative broadband coherent optical sources

One disadvantage of the PCF used in this study is that the bandwidth of the scalar GNLSE-quantified fiber continua is limited to ~ 300 nm [Fig. 4(d)]. It is tempting to increase this bandwidth by selecting a longer fiber length. However, this effort has been unsuccessful due to the earlier onset of the nonlinear polarization-mode depolarization in a longer PCF. The experiment of Fig. 3 suggests that a larger unintentional linear birefringence is rather efficient to suppress the nonlinear polarization-mode depolarization. Thus, a polarization-maintaining DFDD-ANDiF with large ($>2 \times 10^{-5}$) built-in linear birefringence could be the ideal candidate for the PCF-based alternative broadband coherent optical sources (Fig. 1), providing the fiber is pumped along one principal axis of the fiber, and preferably, the slow axis. If the simple PCF design of Fig. 1 is used as the starting point, the powerful dispersion-engineering capability of PCFs along with certain intelligent designs may introduce the polarization-maintaining ability through symmetry-broken fiber guiding region, and at the same time, further decrease its normal dispersion, improve the flatness of the dispersion over a wider bandwidth, and increase the nonlinearity of the PCF. In contrast to the well-known dispersion-engineering of ZDW PCFs intended for generating the broadest supercontinuum, this polarization-maintaining DFDD-ANDiF represents another useful dispersion-engineered class of PCFs suitable for coherent continuum generation, leading to alternative broadband coherent optical sources with scalar GNLSE-quantified spectral-temporal properties. It should be noted that the continuum generation from the polarization-maintaining DFDD-ANDiF does not necessarily produce the fringed spectra of Fig. 4. Flat-top smooth continuum generation with broader bandwidths can be achieved if shorter incident laser pulses or longer fiber lengths are used [16]. In this case, however, the fringed continuum generation at a short fiber length (Fig. 4) may still be useful to validate the scalar GNLSE-based quantification, which would be difficult for the featureless smooth continuum generation.

While the above route intentionally introduces a large linear birefringence to suppress the weak unintentional intrinsic birefringence of the PCF (and the corresponding nonlinear polarization-mode depolarization), an alternative (and seemly opposite) route is to completely avoid the weak unintentional birefringence by choosing fibers with perfect symmetry and with rotation symmetry of order higher than 2 [19], such as circular symmetry [15] and hexagonal symmetry [16]. The fibers of these symmetries are guaranteed to be non-birefringent [19], so that the fibers pumped by linearly polarized pulses can be effectively treated as polarization-maintaining fibers where the scalar GNLSE is valid [15,16]. This alternative route, although theoretically plausible, could be practically difficult. First, it is challenging to fabricate fibers with low ($<10^{-8}$) birefringence, so that the effect of nonlinear polarization-mode depolarization could be persistent. Second, the incident pulses could be slightly elliptical to excite the two degenerate polarization modes of a strictly non-birefringent fiber, so that the fiber output could be depolarized by cross-phase modulation [28].

6. Conclusions

A highly polarized fiber continuum source that can be rigorously quantified by the scalar GNLSE has been constructed using commercially available components. Due to the relatively high spectral density (1 mW/nm), long fiber length (90 mm), long pump pulse width (229 fs FWHM), and most importantly, the fully characterized pulse envelope, this source could be useful in applications where broadband ultrashort (<15 fs) pulse compression/shaping is required. Nonlinear polarization-mode depolarization is identified as the key factor that limits the bandwidth of the current source. Improved polarization-maintained fiber design should overcome this limiting factor to result in a series of attractive alternative broadband coherent optical sources based on birefringent DFDD-ANDiF. The corresponding scalar GNLSE-quantified fiber continua can guide the pulse compression procedure necessary for ultra-broadband coherent control in ultrafast spectroscopy and microscopy.

Acknowledgments

This work was supported in part by grants from the National Institutes of Health (NIH) (NCI R33 CA115536; NIBIB R01 EB009073; NCI RC1 CA147096, S.A.B.). Additional information can be found at <http://biophotonics.illinois.edu>.